IIETA International Information and Engineering Technology Association
Advancing the World of Information and Engineering

Journal Européen des Systèmes Automatisés
Vol. 58, No. 11, November, 2025, pp. 2243-2250
Journal homepage: http://iieta.org/journals/jesa

Robust Multivariable Control of a PMSM Via μ-Synthesis Under Structured Parametric Uncertainties

Farid Oudjama[1,2*], Mohammed Messirdi[2], Khayreddine Saidi[2,3], Abdelmadjid Boumediene[2]

[1] Higher School of Applied Sciences of Tlemcen, Tlemcen 13000, Algeria
[2] Laboratory of Automatic of Tlemcen (LAT), University of Tlemcen, Tlemcen 13000, Algeria
[3] Electrical Engineering Faculty, Djillali Liabes University, Sidi Bel Abbes 22000, Algeria

Corresponding Author Email: faridoudjama@gmail.com

https://doi.org/10.18280/jesa.581103

Received: 28 August 2025
Revised: 18 November 2025
Accepted: 22 November 2025
Available online: 30 November 2025

Keywords:
robust control, multivariable control, PMSM, FOC, μ-synthesis, structured uncertainties, MIMO model, frequency weighting functions

ABSTRACT

This study introduces a robust multivariable control approach for a permanent magnet synchronous motor (PMSM), designed to maintain stability and performance despite parametric uncertainties. A multi-input multi-output (MIMO) model of the PMSM is established in the (d,q) reference frame, leveraging field-oriented control (FOC) to effectively decouple the d- and q-axis dynamics. Six key parameters stator resistance, d- and q-axis inductances, magnetic flux linkage, moment of inertia, and viscous friction are treated as uncertain, with variations up to ±30%. The controller is developed using μ-synthesis within the $H\infty/\mu$ framework, incorporating diagonal frequency weighting functions to balance performance, disturbance rejection, and control effort. A D-K iteration process is employed to derive a reduced-order controller, ensuring robust stability across the uncertainty range. Simulations in Simulink validate the controller's effectiveness in tracking references and rejecting disturbances. This work demonstrates the efficacy of μ-synthesis for robust PMSM control in challenging, uncertain conditions.

1. INTRODUCTION

The robust control of nonlinear electromechanical systems in the presence of structured parametric uncertainties is a fundamental research area in modern control engineering. Among these systems, the permanent magnet synchronous motor (PMSM) plays a central role in high-performance industrial applications such as electric vehicles, drones, industrial robots, and aerospace propulsion systems, due to its excellent torque-to-weight ratio, high efficiency, and fast dynamics [1-3]. However, the performance of these systems strongly depends on the accuracy of the model used for controller design. In practice, the physical parameters of the PMSM—namely stator resistance R_s, d- and q-axis inductances L_d and L_q, magnet flux linkage ϕ_f, mechanical inertia J_m, and viscous friction coefficient B are subject to significant variations due to temperature, magnetic saturation, mechanical wear, or material aging [4-6]. These variations compromise the stability and performance of classical field-oriented control (FOC) strategies based on PI regulators, which are designed for a nominal model and exhibit limitations under severe parametric uncertainties, such as overshoot, steady-state error, and poor disturbance rejection [7-9]. To overcome these limitations, several advanced approaches have been proposed, such as adaptive control, fuzzy logic, or model predictive control [10-12]. However, these methods often lack formal guarantees of robust stability. In contrast, robust control based on the $H\infty/\mu$ framework provides a mathematically rigorous approach to designing controllers capable of maintaining performance and stability under structured uncertainties [13, 14]. Unlike standard $H\infty$ synthesis, which treats uncertainties as unstructured, μ-synthesis exploits their physical nature (real, bounded, decoupled parameters), thereby reducing the conservatism of the solution and providing finer robustness guarantees [15, 16].

The field of robust PMSM control has been the subject of extensive research aimed at improving stability and performance under parametric uncertainties and exogenous disturbances. Several studies have used synthesis and μ-analysis to guarantee robust stability and disturbance rejection under severe parameter variations [17, 18]. Others have explored nonlinear strategies such as backstepping control [19], finite-control-set model predictive control (FCS-MPC) [20, 21], or disturbance-observer-based adaptive control [22, 23]. Recent works have demonstrated the effectiveness of robust MIMO control for electric motor drives under parametric uncertainties, as well as the importance of frequency weighting functions for disturbance rejection. These contributions confirm the relevance of μ-synthesis for multivariable electromechanical systems [24-27].

In this work, we propose a MIMO model of the PMSM with two inputs u_d, u_q (axis voltages) and two outputs, i_d, ω_m (axis current and mechanical speed), developed in the (d,q) frame by exploiting FOC to ensure effective decoupling between the d and q axes. This model, although simplified, captures the dominant dynamics of the PMSM and constitutes a solid basis for the synthesis of a robust controller. Six

physical parameters (R_s, L_d, L_q, ϕ_f, J_m, B) are modeled as uncertain with ±30% variations, reflecting real operating conditions [4, 5].

The μ-synthesis framework combines robust control design and μ-analysis to synthesize a controller that ensures both nominal performance and robust stability in the presence of structured uncertainties. A robust controller is then obtained via a D-K iteration procedure, which alternates between an $H\infty$ synthesis step (K-step) and a scaling analysis step (D-step) to minimize μ over the entire frequency range of interest. This approach has been successfully applied to complex systems such as altitude test facilities and electromechanical drives under load disturbances, demonstrating its ability to ensure precise tracking and excellent disturbance rejection even under fast commands and strong perturbations [24-27].

A generalized MIMO plant is constructed, and a μ synthesis with diagonal weighting functions is implemented via a D-K iteration, yielding a reduced-order controller. The weighting functions are chosen to reflect performance, disturbance rejection, and control effort objectives, in accordance with the mixed-sensitivity loop-shaping structure. The controller obtained from the D-K algorithm is typically high-order. To facilitate implementation, order reduction is performed via modal approximation while preserving robust stability properties [26, 27].

The resulting controller is validated through simulation, demonstrating its effectiveness in reference tracking and disturbance rejection. The results show that the closed-loop system maintains a stable and accurate dynamic response, even under severe parametric variations, as encountered in real operating conditions. This study confirms the effectiveness of μ-synthesis for robust PMSM control in uncertain environments.

2. MULTIVARIABLE MODELING OF THE PMSM IN THE (d,q) REFERENCE FRAME

The synthesis of a robust multivariable controller for the PMSM relies on a global dynamic model of the system, integrating both electrical and mechanical dynamics. The model is established in the rotating (d,q) reference frame, where three-phase quantities are transformed into continuous signals via the park transformation. The basic equations are [1, 9, 17]:

$$\begin{aligned} u_d &= R_s i_d + L_d \frac{di_d}{dt} - \omega_e L_q i_q \\ u_q &= R_s i_q + L_q \frac{di_q}{dt} + \omega_e L_d i_d + \omega_e \phi_f \\ J_m \frac{d\omega_m}{dt} &= T_e - T_l - B\omega_m \end{aligned} \quad (1)$$

where, the electromagnetic torque is:

$$T_e = \frac{3}{2} p\left[\phi_f i_q + \left(L_d - L_q\right) i_d i_q\right]$$

The terms $\omega_e L_q i_q$ and $\omega_e L_d i_d$ induce strong cross coupling between the d- and q-axes. In FOC, this coupling is typically mitigated by feedforward compensation embedded in high bandwidth current regulators. Under the common assumption $i_d = 0$ (MTPA strategy), torque reduces to $T_e = \frac{3}{2} p \phi_f i_q$, enabling near-independent regulation of flux and torque provided the machine parameters(L_d, L_d, ϕ_f) are accurately known and the current loops are sufficiently fast to ensure time-scale separation.

However, this simplification warrants careful qualification. At high speeds, the coupling terms grow linearly with rotor speed; even modest parameter errors lead to residual cross coupling, which may manifest as torque ripple, degraded transient tracking, or phase lag. Under heavy-load conditions, large i_q values exacerbate sensitivity to inductance mismatches, and small deviations from $i_d = 0$ arising from inverter saturation, sensor noise, or finite control bandwidth can re-excite inter-axis dynamics. Near voltage or current limits, standard linear compensation may no longer be adequate, and the assumption of perfect decoupling can compromise both performance and closed-loop stability [1, 7, 8].

Under these assumptions, the channels $u_d \rightarrow i_d$ and $u_q \rightarrow i_q$ become independent. The first is described by:

$$G_{i_d}(s) = \frac{I_d(s)}{U_d(s)} = \frac{1}{L_d s + R_s} \quad (2)$$

The second results from the cascade: voltage $u_q \rightarrow$ current $i_q \rightarrow$ torque $T_e \rightarrow$ speed ω_m:

$$G_\omega(s) = \frac{\Omega_m(s)}{U_q(s)} = \frac{3p\phi_f}{(Js + B)\left(L_q s + R_s\right)} \quad (3)$$

The global system is then represented by a diagonal MIMO transfer matrix:

$$G(s) = \begin{bmatrix} \frac{1}{L_d s + R_s} & 0 \\ 0 & \frac{3p\phi_f}{(Js + B)\left(L_q s + R_s\right)} \end{bmatrix} \quad (4)$$

where, $u = \left[u_d, u_q\right]^T$ and $y = [i_d, \omega_m]^T$. Although simplified, this model captures the dominant dynamics of the PMSM and provides a sound basis for robust controller synthesis via μ-synthesis [25, 27], as long as the design explicitly incorporates margins for parametric uncertainty and residual coupling, especially near the boundaries of the operational envelope.

3. CONTROLLER SYNTHESIS VIA μ-SYNTHESIS

3.1 Robustness problem formulation

The design of a robust controller for the PMSM relies on the μ −synthesis framework, a rigorous method to ensure both robust stability and nominal performance in the presence of structured parametric uncertainties [24, 25-27]. The nominal model $G(s)$, established in the previous section, is augmented with a structured uncertainty block Δ, grouping variations in the six physical parameters: stator resistance R_s, inductances L_d, L_q, magnet flux ϕ_f, inertia J_m, and viscous friction B. Each uncertainty is modeled as a normalized multiplicative perturbation bounded in $H\infty$ norm:

$$p = p_0(1 + \delta_p \Delta_p), \left|\Delta_p\right| \leq 1$$

where, p_0 is the nominal value, δ_p the uncertainty level (e.g., 0.3 for ±30%), and Δ_p a normalized variable. This structure captures the combined effects of parametric variations while preserving system causality [26, 27].

3.2 Structure and generalized plant

The fundamental structure of μ-synthesis relies on the Linear Fractional Transformation (LFT) (Figure 1), which separates the system into two parts: a nominal model P(s) and a structured uncertainty block Δ. The controller $K(s)$ is interconnected via a lower LFT (LLFT), while the uncertainty block is connected via an upper LFT (ULFT) [25-27].

The generalized plant $P(s)$ is described in state-space form as:

$$P_\Delta: \begin{pmatrix} x(t) \\ v(t) \\ z(t) \\ y(t) \end{pmatrix} = \begin{pmatrix} A & B_d & B_w & B_u \\ C_v & D_{vd} & D_{vw} & D_{vu} \\ C_z & D_{zd} & D_{zw} & D_{zu} \\ C_y & D_{yd} & D_{yw} & D_{yu} \end{pmatrix} \begin{pmatrix} x(t) \\ d(t) \\ w(t) \\ u(t) \end{pmatrix} \quad (5)$$

where:

- $x(t)$: system state,
- $d(t)$: exogenous disturbances (uncertainties, noise),
- $w(t)$: reference signals,
- $u(t)$: control input,
- $v(t)$: output of the uncertainty block Δ,
- $z(t)$: weighted output (performance),
- $y(t)$: measurement.

The ULFT interconnection between Δ_p and Δ is defined by:

$$\begin{gathered} v = P_{11}d + P_{12}w, w = P_{21}d + P_{22}w, d = \Delta v \\ \Rightarrow z = \mathrm{ULFT}(P_\Delta, \Delta)w \end{gathered} \quad (6)$$

The LLFT interconnection between P_Δ and K is defined by:

$$\begin{gathered} u = P_{12}K(I - P_{22}K)^{-1}P_{21}w + P_{11}\mathrm{w} \\ \Rightarrow z = \mathrm{LLFT}(P_\Delta, \Delta)w \end{gathered} \quad (7)$$

Figure 1 illustrates this standard interconnection [1].

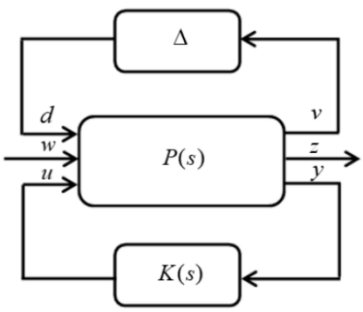

Figure 1. Generalized plant interconnection with the controller and uncertainty blocks [26, 27]

3.3 Definition and interpretation of the structured singular value (μ)

The structured singular value μ, or structured singular value, is a fundamental measure of robustness of a closed-loop system in the presence of structured uncertainties [24, 25, 27]. For a closed-loop system represented by the transfer function $T_{zw}(s) = \mathrm{LLFT}(P_\Delta, K)(s)$, μ is defined as:

$$\mu_\Delta(T_{zw}(jw)) = \left(\min_{\Delta \in \mathbf{\Delta}} \left(\frac{\bar{\sigma}(\Delta)}{\det(I - T_{zw}(jw)\Delta)} = 0\right)\right)^{-1} \quad (8)$$

The system is robustly stable if and only if:

$$\sup_{\omega \in R} \mu_\Delta(T_{zw}(j\omega)) < 1 \quad (9)$$

This condition ensures closed-loop stability even under extreme parametric variations. An upper bound of μ is given by:

$$\mu_\Delta(T_{zw}(j\omega)) \leq \inf_{D \in \boldsymbol{D}} \bar{\sigma}(D(j\omega)T_{zw}(j\omega)D^{-1}(j\omega)) \quad (10)$$

where, D is the set of scaling matrices compatible with the structure of D [8]. This bound is minimized during the D-K iteration.

3.4 Frequency weighting functions and MIMO structure

A generalized plant $P(s)$ is constructed using frequency weighting functions to formulate a mixed-sensitivity control problem. These weights are chosen to reflect design objectives [24, 25, 27].

- $W_1(s)$: sensitivity weighting, shaping tracking accuracy and low-frequency disturbance rejection,
- $W_2(s)$: control effort weighting, limiting actuator demand and preventing inverter saturation,
- $W_3(s)$: complementary sensitivity weighting, ensuring robustness against unmodeled dynamics (e.g., residual coupling, fast parameter variations, high-frequency noise).

These functions are defined as diagonal matrices:

$$\begin{aligned} W_1(s) &= \mathrm{diag}\big(W_{1,i_d}(s), W_{1,\omega}(s)\big) \\ W_2(s) &= \mathrm{diag}\big(W_{2,i_d}(s), W_{2,\omega}(s)\big) \\ W_3(s) &= \mathrm{diag}\big(W_{3,i_d}(s), W_{3,\omega}(s)\big) \end{aligned} \quad (11)$$

Each element is a stable, minimum-phase first-order filter, designed to jointly achieve:

- high gain at low frequencies for precise tracking and disturbance rejection,
- controlled roll-off to limit closed-loop bandwidth and avoid noise amplification,
- bounded high-frequency gain to constrain control effort.

The diagonal structure of the weights is justified by the decoupled nature of the PMSM multivariable model in the (d,q) frame. After FOC, the d and q axes are nearly independent: i_d primarily controls flux, while i_q controls torque. This separation allows diagonal weighting, simplifying controller synthesis while maintaining satisfactory performance [24, 26]. It also reduces computational complexity and avoids convergence issues associated with full matrices.

The tuning process is systematic and iterative: first, frequency domain constraints are enforced to guarantee robust stability and performance margins; second, time-domain validation under representative operating conditions confirms

satisfactory dynamic response, disturbance rejection, and control authority. This two-stage approach ensures that the weighting functions translate high-level design requirements precision, robustness, and real time implement ability into mathematically tractable specifications for μ-synthesis.

Figure 2 shows the block diagram of the proposed experiment, where the augmented plant is fed only by reference signals. This structure simplifies analysis and synthesis by focusing all performance objectives on reference response [27].

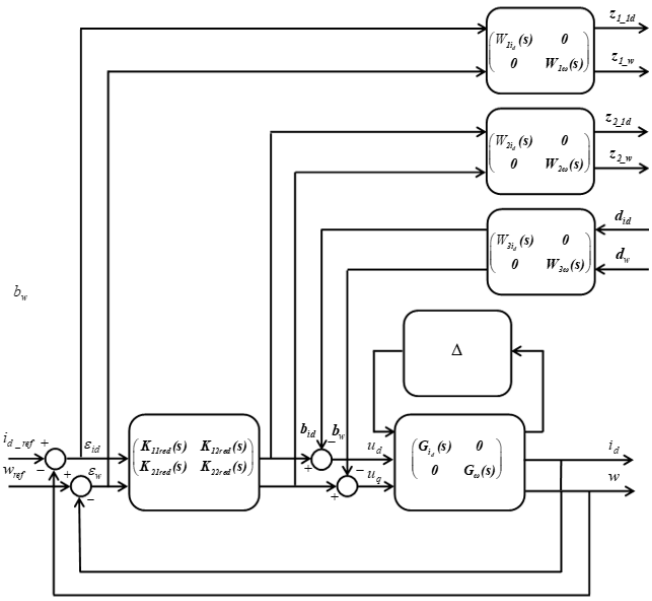

Figure 2. The block diagram of the proposed experiment containing the augmented plant which contains as inputs the reference signals only

3.5 D-K iteration algorithm

μ-synthesis cannot be solved directly because the structured singular value μ is not a convex norm. An effective solution is the D-K iteration algorithm, which alternates between two steps:

1. K-step ($H\infty$ Synthesis): With fixed scaling matrices $D(j\omega)$, solve a standard $H\infty$ problem. Find a controller $K(s)$ minimizing the norm of the scaled system $H \propto \|D(s)T_{zw}(s)D^{-1}(s)\|_{\infty}$ [13].
2. D-step (μ-Analysis): With fixed controller $K(s)$, compute at each frequency ω a scaling matrix $D(j\omega)$ that minimizes the largest singular value of the scaled system: $\min_{D} \bar{\sigma}(D(j\omega)T_{zw}(j\omega)D^{-1}(j\omega))$ then interpolate the $D(j\omega)$ by a stable, minimum-phase system.

The D and K steps are iterated until convergence, i.e., until $\mu < 1$ over the entire frequency range of interest [25, 27].

4. SIMULATION RESULTS

The PMSM under study is a 20-kW machine designed for high-performance industrial applications. The complete set of its electrical and mechanical parameters is summarized in Table 1. The robust multivariable controller was designed using μ-synthesis, a powerful framework for handling structured uncertainties. The design process began with the formulation of an uncertain MIMO model in the (d,q) reference frame, where six key parameters, L_d, L_q, ϕ_f, J_m, and B were treated as uncertain, with variations of up to ±30%. This uncertainty model reflects real-world operating conditions such as temperature drift and component aging.

The robust controller obtained through the D–K iteration procedure initially results in a high-order design (71 states), which is a common outcome when structured uncertainties are explicitly incorporated within the μ-synthesis framework. To mitigate this complexity while retaining the essential closed-loop characteristics, a balanced-truncation–based order reduction was subsequently performed. Several reduced-order candidates were generated and assessed. The fidelity of each reduced model was quantified by computing the H∞ norm of the approximation error between the full-order controller and its reduced counterpart. Among the examined orders, the sixth-order model provided the most favorable trade-off. The associated H∞ error, equal to 7.29×10^{-3}, is remarkably small, indicating that the dominant dynamical features are effectively preserved. This conclusion is further supported by the Hankel singular value distribution, which exhibits a pronounced drop beyond the sixth mode, confirming that the truncated states contribute negligibly to the input–output behavior. Post-reduction μ-analyses, together with time-domain simulations under severe parametric variations and transient load disturbances, demonstrate that the reduced controller maintains the robustness and performance properties of the full-order design. The final controller is expressed as a 2 × 2 transfer function matrix, providing a compact and structurally consistent representation well suited for multivariable robust control of the PMSM under uncertain operating conditions.

$$K_{\mu} = \left[\begin{pmatrix} K_{11\,\mathrm{red}}(s) & K_{12\,\mathrm{red}}(s) \\ K_{21\,\mathrm{red}}(s) & K_{22\,\mathrm{red}}(s) \end{pmatrix}\right] \tag{12}$$

where, each element is a sixth-order transfer function derived from the reduction process, preserving the robust performance characteristics of the full-order design.

Table 1. Parameters of the PMSM model [28]

Parameter	Symbol	Value
Nominal power	P_n	20 kW
Nominal speed	N_n	1500 rpm
Number of pole pairs	P	4
Magnetic flux linkage	ϕ_f	0.19 Wb
d-axis inductance	L_d	1.475 mH
q-axis inductance	L_q	1.6 mH
Stator resistance	R_s	15 mΩ
Rotor inertia	J_m	0.05 kg·m²
Viscous friction coefficient	B	0.0012 N·m·s/rad

The robust stability analysis yields a peak structured singular value of only 0.39, as shown in Figure 3, confirming internal stability over the full set of structured uncertainties typical of permanent-magnet synchronous motors, including temperature-dependent flux weakening, thermal drift of stator resistance, and inductance variations due to magnetic saturation or rotor position. This comfortable margin stems from a deliberately balanced weighting design: $W_1(s)$, acting on the tracking error, ensures steady-state accuracy below 1% and effective low-frequency disturbance rejection, while

$W_2(s)$, acting on the control signal, constrains high-frequency actuation to preserve phase margin and avoid exciting unmodeled dynamics such as PWM harmonics or sensor delays. Pushing for faster nominal response—by increasing the low-frequency gain of $W_1(s)$ or relaxing the roll-off $W_2(s)$ of raises the structured singular value toward the critical threshold of 1, whereas overly conservative tuning degrades responsiveness. The selected configuration thus achieves a certified trade-off between precision, speed, and robustness a trade off particularly well suited to the PMSM, whose structural simplicity (negligible saliency, weak d-q coupling) inherently enables both high bandwidth and manageable parametric sensitivity, provided the controller synthesis explicitly accounts for its dominant uncertainty sources.

The robust performance analysis, presented in Figure 4, shows that the peak value of $\mu(\Delta)$ is 0.97, which is also below 1. This confirms that the closed-loop system meets all performance specifications reference tracking, disturbance rejection, and noise attenuation even under the most adverse conditions. This value of 0.94 reflects a deliberate trade-off in the weighting function design: increasing the low-frequency gain of $W_1(s)$ (to improve tracking and disturbance rejection) or reducing the high-frequency roll-off of $W_3(s)$ (to extend bandwidth) would raise the peak μ_Δ, pushing it closer to the critical threshold of 1 and thereby eroding robustness margins. Conversely, more conservative weights would enhance robustness at the expense of nominal performance (e.g., larger steady-state error, slower response). The selected weights thus represent an optimal balance: they ensure effective load disturbance rejection and steady-state error below 1 %, while preserving sufficient robustness margins as validated in Figure 4 to guarantee stability and performance across the full operational envelope.

The controller's performance was validated through extensive simulations in Simulink. The test scenario includes a startup phase, a speed inversion, and the application of a mechanical load. As shown in Figure 5, the motor reaches the reference speed of 157 rad/s (1500 rpm) quickly and without overshoot. At t = 6 s, a speed inversion is commanded, switching from +157 rad/s to -157 rad/s. The transition is smooth and rapid, with no oscillations or instability, demonstrating excellent regulation in both motoring and generating modes.

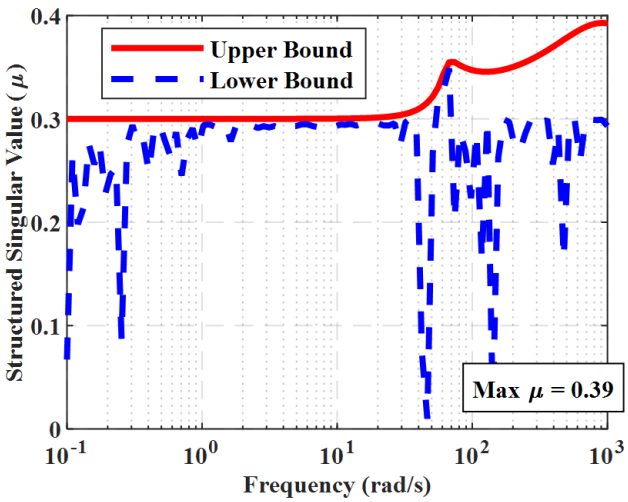

Figure 3. Robust stability analysis

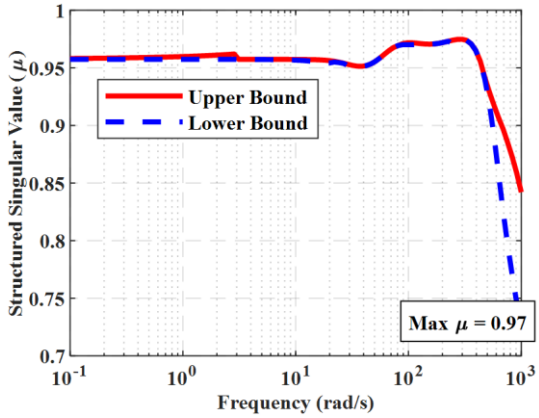

Figure 4. Robust performance analysis

At t = 12 s, a load torque of 20 N·m is abruptly applied. As Figure 5 clearly shows, no speed drop is observed. The system maintains the reference speed of -157 rad/s with zero steady-state error, showcasing exceptional disturbance rejection and robustness.

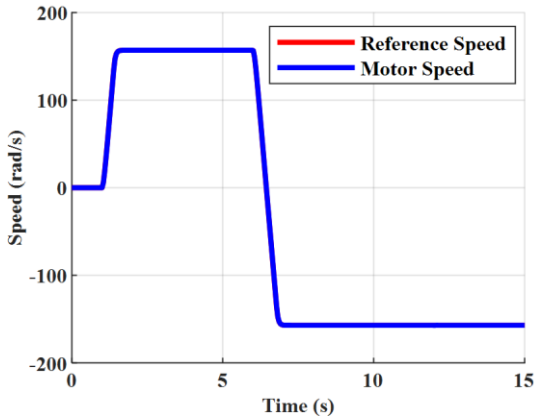

Figure 5. Motor speed response

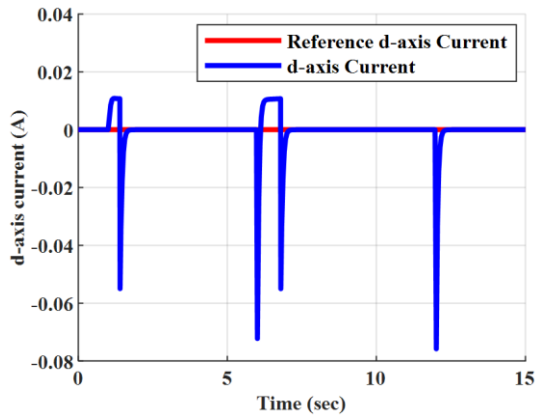

Figure 6. d-axis current response

Figure 6 displays the d-axis current i_d. It is tightly regulated around zero throughout the simulation, with only negligible transient variations. This behavior confirms effective flux regulation, which is a cornerstone of field-oriented control.

Figure 7 shows the q-axis current i_q. In steady state, it stabilizes at a constant value. Crucially, at t = 6 s, when the speed inversion occurs, i_q abruptly changes sign, transitioning from positive to negative to generate the torque required for

deceleration and subsequent acceleration in the reverse direction. This sharp, well-damped transition highlights the controller's precise and immediate response to demanding dynamic commands.

Figure 8 presents the electromagnetic torque response. The torque quickly reaches its reference value at startup, with an initial peak of 20 N·m. At t = 6 s, it changes sign smoothly to facilitate the speed inversion. At t = 12 s, it increases to counteract the applied load, all without saturation or oscillation. This linear and controlled response confirms the controller's ability to manage complex, multi-event scenarios with high fidelity.

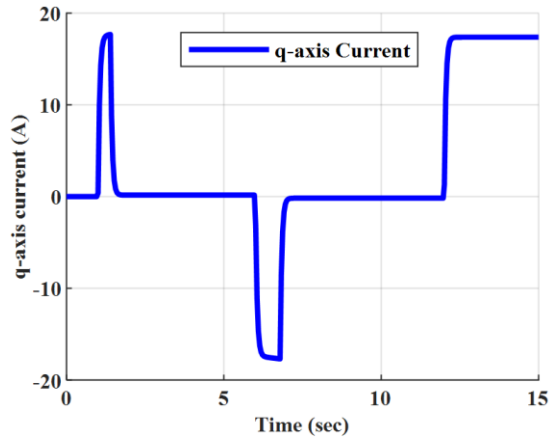

Figure 7. q-axis current response

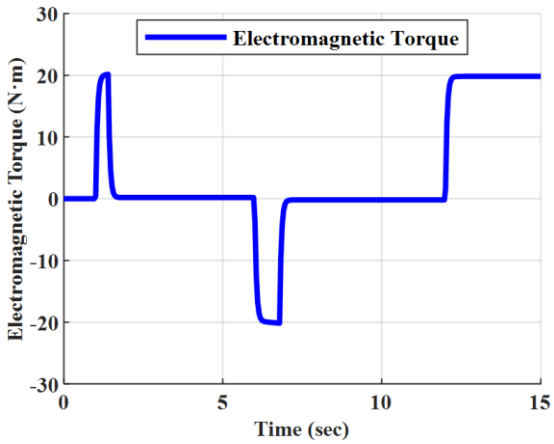

Figure 8. Electromagnetic torque response

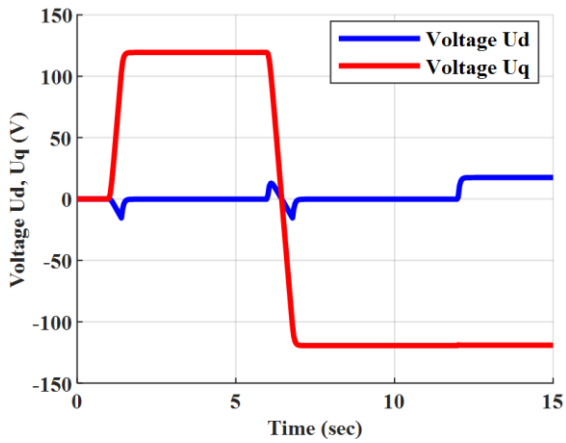

Figure 9. d and q axis voltage commands

Figure 9 shows the d- and q-axis voltage commands. Despite an aggressive speed reversal at 6 s and a sudden +20 N·m load torque step at 12 s, both control voltages remain strictly within the admissible operating range of a standard industrial inverter, with no saturation observed. This confirms that the control effort weighting matrix $W_2(s)$ successfully enforces actuator constraints by design, while preserving high dynamic responsiveness—a critical requirement for the real-world deployment of robust multivariable controllers.

Figure 10 illustrates the speed response under extreme parametric uncertainty, with variations reaching plus or minus one hundred percent on stator resistance and inductance. These ranges capture not only severe thermal drift and manufacturing dispersion, but also critical fault scenarios such as partial winding short circuits or deep magnetic saturation. Across all cases, the system achieves precise reference tracking, zero steady-state error, and fast, well-damped transients—without instability or performance degradation. This behavior demonstrates that μ-synthesis, when combined with a balanced weighting of tracking error, control effort, and input disturbance, delivers guaranteed stability and high nominal performance, even well beyond standard operating conditions.

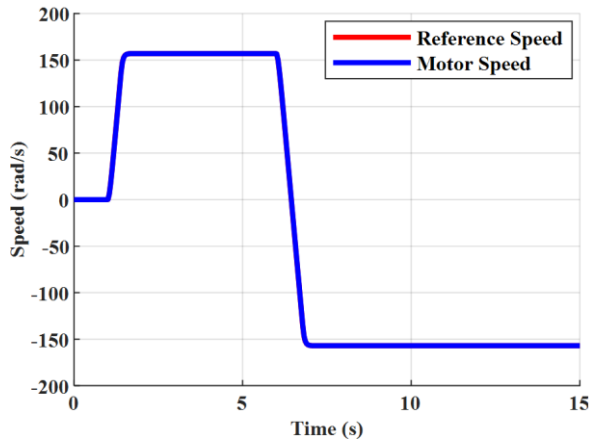

Figure 10. Robust speed tracking under time-varying stator resistance and inductances

To contextualize the performance of the proposed controller, a comparison is made with the high-performance sliding-mode approach recently reported in a study [29]. Under nominal conditions, the μ-synthesis controller achieves a rise time of 0.12 s (vs. 0.18–0.22 s), zero overshoot (vs. 2–5 %), and a disturbance rejection time of 5 ms (vs. 80–120 ms), while maintaining zero steady-state error—these results are summarized in Table 2. More importantly, under extreme structured uncertainties (±100 % stator resistance, ±100 % inductance), it guarantees internal stability and performance preservation by construction of the structured singular value framework—whereas the sliding-mode controller in the study [29] provides no such formal robustness certificate. This demonstrates that the proposed method ensures not only fast and precise tracking for the MSAP, but also certified robustness against severe parametric drift and fault-like conditions, a decisive advantage for high-reliability permanent-magnet drives.

In summary, the simulation results demonstrate that the μ-synthesis-based controller, even after order reduction, delivers high dynamic performance, precise current regulation, perfect speed tracking, and outstanding robustness against parametric uncertainties and external disturbances.

Table 2. Comparative performance: μ-synthesis vs. sliding-mode control [29]

Performance Metric	Sliding Mode [19]	Proposed μ-Synthesis
Rise time (s)	0.18 – 0.22	0.12
Overshoot (%)	2 – 5	0
Steady state error	0	0
Disturbance rejection (ms)	80 – 120	5
Certified robustness	No	Yes

5. CONCLUSION

This paper has presented a robust multivariable control strategy for a PMSM based on μ-synthesis, specifically designed to maintain high performance under significant structured parametric uncertainties of up to ±30%. A MIMO model was developed in the (d,q) reference frame, leveraging FOC principles to decouple the machine's dynamics. The uncertainties in key parameters—stator resistance, d- and q-axis inductances, magnetic flux, moment of inertia, and viscous friction—were explicitly modeled, allowing for a systematic design process.

The controller was synthesized using the D–K iteration method, resulting in a high-order solution that was subsequently reduced to a practical order of 6 while preserving the critical robustness properties. The final controller requires only the measurement of rotor speed, simplifying the sensor requirements and the overall control architecture.

Simulation results in Simulink demonstrate the controller's exceptional performance. It achieves precise speed tracking, maintains zero d-axis current for optimal flux regulation, and exhibits an immediate and robust response to both speed inversions and load torque disturbances. The complete absence of speed drop under load and the seamless transition during speed reversal underscore the controller's robustness.

This work demonstrates the significant potential of μ-synthesis for robust PMSM control in challenging, real-world conditions where parameter variations are inevitable. The approach provides a rigorous, model-based alternative to conventional control methods, ensuring stability and performance guarantees across the entire uncertainty domain. The successful validation of the reduced-order controller highlights its practical feasibility for industrial applications such as electric vehicles, robotics, and precision drives.

Nevertheless, the validity of the proposed approach is bounded by two key assumptions. First, it relies on an accurate machine model and effective d q axis decoupling via field-oriented control. This assumption may be challenged under extreme operating conditions, particularly when significant thermal effects alter the stator resistance and permanent magnet flux, or when unmodeled nonlinearities such as magnetic saturation and inverter dead time effects become dominant. Second, while the sixth order realization is theoretically suitable for embedded implementation, critical real time constraints, including computational load, execution latency, and minimum sampling frequency have not yet been quantified and will be rigorously assessed during experimental validation.

Future work will focus on experimental validation of the controller on a physical test bench. This will provide further evidence of its real-time performance and robustness. Additionally, the integration of this control strategy with advanced techniques like field-weakening control will be explored to extend the operational speed range of the motor.

ACKNOWLEDGMENT

The DG RSDT (Direction Générale de la Recherche Scientifique et du Développement Technologique) supported this work.

REFERENCES

[1] Ullah, K., Guzinski, J., Mirza, A.F. (2022). Critical review on robust speed control techniques for permanent magnet synchronous motor (PMSM) speed regulation. Energies, 15(3): 1235. https://doi.org/10.3390/en15031235

[2] El Fakir, C., El Idrissi, Z., Lassioui, A., Belhaj, F.Z., Gaouzi, K., El Fadil, H., Rachid, A. (2023). Adaptive nonlinear control of salient-pole PMSM for hybrid electric vehicle applications: Theory and experiments. World Electric Vehicle Journal, 14(2): 30. https://doi.org/10.3390/wevj14020030

[3] Kasri, A., Ouari, K. (2024). Robust intelligent nonlinear predictive control based on artificial neural network for optimizing PMSM drive performance. Periodica Polytechnica Electrical Engineering and Computer Science, 68(4): 37217. https://doi.org/10.3311/PPee.37217

[4] Yuan, T., Chang, J., Zhang, Y. (2023). Parameter identification of permanent magnet synchronous motor with dynamic forgetting factor based on H∞ filtering algorithm. Actuators, 12(12): 453. https://doi.org/10.3390/act12120453

[5] Cao, G., Chen, Z., Wang, D., Zhao, X., Meng, F. (2025). A robust fuzzy adaptive control scheme for PMSM with sliding mode dynamics. Processes, 13(8): 2635. https://doi.org/10.3390/pr13082635

[6] Li, H., Jian, X. (2023). Parameter identification of permanent magnet synchronous motor based on CGCRAO algorithm. IEEE Access, 11: 124319-124330. https://doi.org/10.1109/ACCESS.2023.3330495

[7] Zhang, L., Ma, J., Wu, Q., He, Z., Qin, T., Chen, C. (2023). Research on PMSM speed performance based on fractional order adaptive fuzzy backstepping control. Energies, 16(19): 6922. https://doi.org/10.3390/en16196922

[8] Bu, Z., Niu, P., Guo, X., He, J. (2024). Fuzzy PID control of permanent magnet synchronous motor electric steering engine by improved beetle antennae search algorithm. Scientific Reports, 14: 2898. https://doi.org/10.1038/s41598-024-52600-8

[9] Yao, X. (2023). Overview of predictive control technology for permanent magnet synchronous motor systems. Applied Sciences, 13(10): 6255. https://doi.org/10.3390/app13106255

[10] Bouguenna, I. F., Benkaihoul, S., Benmadani Debbat, M., Zabel, A., Tahour, A. (2025). Sliding mode predictive control using model reference adaptive system of permanent magnet synchronous motor. Wseas Transactions on Electronics, 16(3): 22-32. https://doi.org/10.37394/232017.2025.16.3

[11] Bu, W., Guo, S., Fan, Z., Li, J. (2025). Improved adaptive

PI-like fuzzy control strategy of permanent magnet synchronous motor. Energies, 18(2): 362. https://doi.org/10.3390/en18020362
[12] Zhou, Y., Huang, C., Li, B. (2023). Speed control of PMSM based on fuzzy ADRC under small disturbances. Applied Sciences, 13(19): 10775. https://doi.org/10.3390/app131910775
[13] Tahami, H., Saberi, S., Ali, B. M., AbdulAmeer, S., Abdul Hussein, A., Chaoui, H. (2024). A robust H∞ based state feedback control of permanent magnet synchronous motor drives using adaptive fuzzy sliding mode observers. Actuators, 13(8): 307. https://doi.org/10.3390/act13080307
[14] Zhou, Y. (2025). A robust recursive feasibility based MPC method for the speed control of uncertain permanent magnet synchronous motors. Journal of Engineering and Applied Science, 72: 155. https://doi.org/10.1186/s44147-025-00724-7
[15] Kasri, Karkkainen, M., Papadimitriou, S. (2024). μ-analysis and μ-synthesis control methods in smart structure disturbance suppression with reduced order control. Algorithms, 17(2): 73. https://doi.org/10.3390/a17020073
[16] Zhang, Q., Yu, R., Li, C., Chen, Y.-H., Gu, J. (2022). Servo robust control of uncertain mechanical systems: Application in a compressor/PMSM system. Actuators, 11(2): 42. https://doi.org/10.3390/act11020042
[17] Elkholy, M.M., Algendy, M. M., El-Hay, E.A. (2025). Modern control techniques and operational challenges in permanent magnet synchronous motors: A comprehensive review. Automation, 6(4): 49. https://doi.org/10.3390/automation6040049
[18] Li, X., Zhang, Y., Wang, H., Chen, J. (2024). Improved current control for PMSM via an active disturbance rejection controller. European Journal of Control, 78: 101005. https://doi.org/10.1016/j.ejcon.2024.101005
[19] Duan, J., Wang, S., Sun, L. (2022). Backstepping sliding mode control of a permanent magnet synchronous motor based on a nonlinear disturbance observer. Applied Sciences, 12(21): 11225. https://doi.org/10.3390/app122111225
[20] Li, T., Sun, X., Yao, M., Guo, D., Sun, Y. (2024). Improved finite control set model predictive current control for permanent magnet synchronous motor with sliding mode observer. IEEE Transactions on Transportation Electrification, 10(1): 699-710. https://doi.org/10.1109/TTE.2023.3293510
[21] Zhang, H., Ran, P., Zhang, Z. (2025). PMSM sensorless control based on super twisting algorithm sliding mode observer with IAORLS parameter estimations. Scientific Reports, 15: 22386. https://doi.org/10.1038/s41598-025-04030-3
[22] Bayir, F., Zergeroğlu, E. (2025). Adaptive backstepping control with real-time fuzzy logic parameter selection of a field-oriented control based PMSM driver. Turkish Journal of Electrical Engineering and Computer Sciences, 33(4): 460-478. https://doi.org/10.55730/1300-0632.4138
[23] Sabouni, E., Merah, B., Bousserhane, I. K. (2021). Adaptive backstepping controller design based on neural network for PMSM speed control. International Journal of Power Electronics and Drive Systems (IJPEDS), 12(3): 1940-1952. https://doi.org/10.11591/ijpeds.v12.i3.pp1940-1952
[24] Skogestad, S., Postlethwaite, I. (2005). Multivariable Feedback Control: Analysis and Design, 2nd ed. Chichester, UK: Wiley.
[25] Duc, G., Font, S. (1999). Commande H∞ et μ-analyse: Des outils pour la robustesse. Paris, France: Hermes Sciences Publications.
[26] Apkarian, P., Noll, D. (2006). Robust Control Design with MATLAB®, 2nd ed. London, UK: Springer.
[27] Roy, T., Barai, R. K. (2022). Robust Control Oriented Linear Fractional Transform Modelling: Applications for the μ-synthesis Based H∞ Control. Springer. https://doi.org/10.1007/978-981-19-7462-5
[28] Krishnan, R. (2010). Permanent Magnet Synchronous and Brushless DC Motor Drives, 1st Edition. eBook published 18 December 2017.
[29] Zhang, Z., Yang, G., Fan, J., Li, T., Cai, Q. (2024). A disturbance sliding mode observer designed for enhancing the LQR current-control scheme of a permanent magnet synchronous motor. Actuators, 13(8): 283. https://doi.org/10.3390/act13080283

NOMENCLATURE

B	Viscous friction coefficient, kg·m²·s⁻¹
$G(s)$	Transfer function matrix of the PMSM, dimensionless
i_d, i_q	d-axis and q-axis stator currents, A
J_m	Rotor inertia, kg·m²
L_d, L_q	d-axis and q-axis inductances, H
P	Number of pole pairs, dimensionless
R_s	Stator resistance, Ω
T_e	Electromagnetic torque, N·m
u_d, u_q	d-axis and q-axis stator voltages, V
ω_m	Mechanical angular speed, rad/s
ω_e	Electrical angular speed, rad/s
ϕ_f	Permanent magnet flux linkage, Wb

Greek symbols

Δ	Block of structured uncertainty, dimensionless
∞	Infinity, dimensionless
μ	Structured singular value, dimensionless

Subscripts

D	d-axis (direct axis)
Q	q-axis (quadrature axis)
S	Stator
E	Electrical
M	Mechanical

Abbreviations

PMSM	Permanent Magnet Synchronous Motor
MIMO	Multiple-Input Multiple-Output
FOC	Field-Oriented Control
$H\infty$	H-infinity control
D–K	Design–K iteration